

Mayer-homology learning prediction of protein-ligand binding affinities

Hongsong Feng¹, Li Shen¹, Jian Liu^{2,1} and Guo-Wei Wei^{*1,3,4}

¹*Department of Mathematics, Michigan State University, East Lansing, MI 48824, USA*

²*Mathematical Science Research Center, Chongqing University of Technology, Chongqing 400054, China*

³*Department of Biochemistry and Molecular Biology, Michigan State University, MI, 48824, USA*

⁴*Department of Electrical and Computer Engineering, Michigan State University, MI 48824, USA*

Abstract

Artificial intelligence-assisted drug design is revolutionizing the pharmaceutical industry. Effective molecular features are crucial for accurate machine learning predictions, and advanced mathematics plays a key role in designing these features. Persistent homology theory, which equips topological invariants with persistence, provides valuable insights into molecular structures. The calculation of Betti numbers is based on differential that typically satisfy $d^2 = 0$. Our recent work has extended this concept by employing Mayer homology with a generalized differential that satisfies $d^N = 0$ for $N \geq 2$, leading to the development of persistent Mayer homology (PMH) theory and richer topological information across various scales. In this study, we utilize PMH to create a novel multiscale topological vectorization for molecular representation, offering valuable tools for descriptive and predictive analysis in molecular data and machine learning prediction. Specifically, benchmark tests on established protein-ligand datasets, including PDBbind-2007, PDBbind-2013, and PDBbind-2016, demonstrate the superior performance of our Mayer homology models in predicting protein-ligand binding affinities.

Key words: Persistent Mayer homology, Machine learning, Protein-ligand binding affinity.

*Corresponding author: weig@msu.edu

1 Introduction

Drug design and discovery is a lengthy and costly process, and the process is plagued by a high failure rate [1]. Developing a new drug can take a decade and cost billions of dollars before it reaches the market. However, the accumulation of extensive experimental biological data and advancements in machine learning algorithms are rapidly transforming AI-based drug design, offering the potential to revolutionize the field. For instance, determining protein–ligand binding affinity is a critical challenge in drug discovery. Machine learning models excel at capturing complex, non-linear relationships in data and provide superior accuracy in predicting binding affinity compared to traditional models [2, 3].

In AI-assisted drug design and discovery, molecular descriptors are crucial to the performance of machine learning models and are integral to various stages of the drug discovery process [4, 5, 6, 7]. They play a fundamental role in quantitative structure–activity relationship (QSAR) [8] and quantitative structure–property relationship (QSPR) analyses [9]. Two-dimensional (2D) and three-dimensional (3D) molecular descriptors are widely used for machine learning predictions. Popular 2D molecular descriptor generation approaches include substructure key-based fingerprints, topological or path-based fingerprints, circular fingerprints, pharmacophore fingerprints [10], and autoencoded fingerprints [11]. These molecular descriptors can typically be extracted from molecular simplified molecular-input line-entry system (SMILES) strings without 3D structure information, and they are primarily used to represent small molecules. However, they do not perform well for macromolecules with complex 3D structures. The 3D molecular descriptors consider molecular structures, as well as chemical, physical, and biological properties [12]. 3D molecular descriptors are superior to 2D ones in scenarios where the three-dimensional structure of a molecule is a key determinant of its biological function, such as protein–ligand interactions, stereochemistry, molecular docking and virtual screening, and conformational analysis. Deep learning methods, such as autoencoders [11], transformers [13], graph neural networks (GNNs) [14], and convolutional neural networks (CNNs) [15, 16, 17], have also been employed for molecular feature generation, producing highly competitive molecular features.

The complexity of biomolecular structure, function, and dynamics often renders structural representation inconclusive, inadequate, inefficient, and, at times, intractable. These challenges necessitate innovative design strategies for representing macromolecules. Recently, advanced mathematical tools such as topological data analysis (TDA) have been employed for biomolecular characterization [18]. These mathematical approaches excel in abstracting and representing intrinsically complex molecular structures, making them particularly suitable for molecular featurization [18, 19]. Although TDA is a relatively new field, it has rapidly emerged as a powerful methodology in data science. The essence of TDA lies in extracting significant topological invariants and geometric shapes, capturing the nuanced patterns and relationships embedded within the data. Persistent homology theory [20, 21, 22, 23] is the primary workhorse in TDA. It utilizes a filtration process that gradually builds up a family of topological spaces from the data by adding simplices (basic geometric shapes like points, edges, triangles, etc.) one at a time, based on parameters such as distance or density. Multiscale representation is reflected in two key aspects: tracking the lifespan of topological invariants across scales—such as connected components, loops, and voids—and describing these invariants, including Betti numbers, which count the number of topological features at different scales. These two aspects are essentially equivalent but provide quantitative analysis

from different perspectives.

Persistent homology is particularly useful for characterizing molecular data and distinguishes itself from traditional molecular descriptors [18]. Its integration with machine learning algorithms has led to significant advancements in various stages of drug design such as predicting protein–ligand binding affinity [18] and changes in protein stability upon mutation [24]. One of the most compelling pieces of evidence for the effectiveness of persistent homology-based molecular descriptors is their significant success in the D3R Grand Challenge [25], a worldwide computer-aided drug discovery competition. The power of TDA is further exemplified in the topological deep learning (TDL) paradigm [18], where topological molecular featurization is integrated with deep neural networks. The early success of mathematical representations and TDL for biomolecular data was documented in a review [26]. Recently, TDL has uncovered the mechanisms of SARS-CoV-2 evolution [27].

Despite its tremendous success, persistent homology theory still faces some drawbacks. Persistent homology can lead to an oversimplification of geometric information from the given data, resulting in a significant loss of crucial details. For example, while it captures cavities and loops, it lacks the precision to describe their shape, depth, or orientation, potentially treating distinct geometries—such as a shallow, wide pocket and a deep, narrow one—as equivalent. To address these limitations, persistent Laplacian theories [28, 29, 30] were introduced. While retaining the ability to capture topological invariants like persistent homology, persistent Laplacians also reveal additional geometric information through the non-harmonic spectrum of their matrices. Their value as molecular descriptors is demonstrated by their accurate forecasting of emerging dominant SARS-CoV-2 variants BA.4/BA.5 [31]. Other valuable topological or geometric data analysis techniques with superb performance include persistent de Rham-Hodge Laplacians [32], and neighborhood path complex [33].

In this study, we explore the potential of persistent Mayer homology (PMH) for characterizing molecules. Unlike usual simplicial homology, which uses a boundary operator d that satisfies $d^2 = 0$, Mayer Homology defined on simplicial complexes employs a boundary operator d where $d^N = 0$ [34]. Mayer Homology reduced to simplicial homology when $N = 2$. The boundary operator is essential for constructing algebraic groups used to identify properties related to connected components, rings, or cavities in simplicial homology. Mayer homology theory provides enhanced Betti number information by varying the value of N , revealing more detailed topological and geometric features of a space [35]. A multiscale topological representation from PMH is obtained through the filtration process, in which a series of nested simplicial complexes is generated. During this process, Betti numbers or the persistence of topological invariants are calculated and used to construct molecular descriptors. These topological features are then combined with a gradient boosting decision tree algorithm to build predictive models. We evaluate the performance of our PMH-based machine learning models on three well-established protein-ligand binding affinity datasets: PDBbind-v2007, PDBbind-v2013, and PDBbind-v2016 [36]. Our models demonstrate exceptional performance, which can be further enhanced by incorporating molecular sequence-based descriptors generated using natural language processing techniques. Compared to the existing literature, our models achieve state-of-the-art performance.

2 Results

2.1 Overview of persistent Mayer homology (PMH)

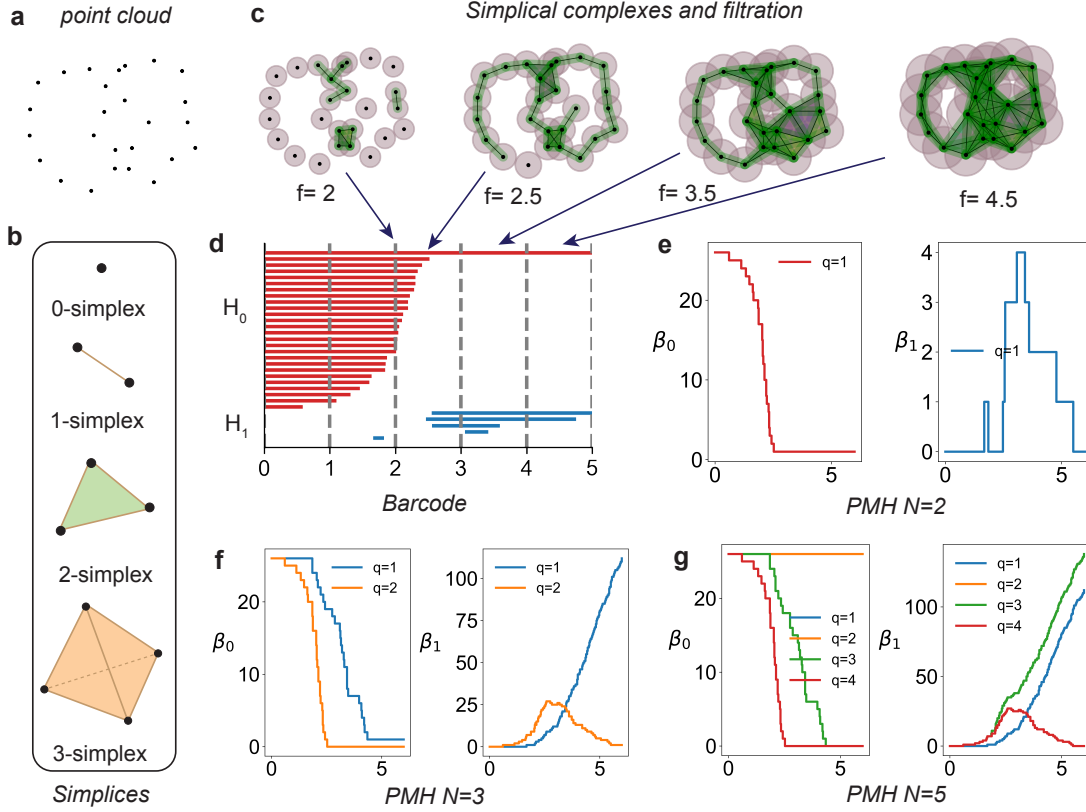


Figure 1: The persistent Mayer homology representation for a point cloud based on VR complex. **a:** A 2D point cloud. **b:** The representation of simplices in dimension $n = 0, 1, 2, 3$. **c:** A filtration of simplicial complexes obtained from the point cloud. **d:** The barcode of dimension 0 and 1 corresponding to the filtration process in **c**. The filtration parameter is defined to be the diameter of circles around given points. **e:** The Betti numbers β_0 and β_1 calculated from persistent Mayer homology (PMH) for $N = 2$. **f:** The Betti numbers β_0 and β_1 calculated from persistent Mayer homology (PMH) for $N = 3$. **g:** The Betti numbers β_0 and β_1 calculated from persistent Mayer homology (PMH) for $N = 5$. The curves at $q = 2$ and $q = 3$ coincides in **g**.

As mentioned early, Mayer homology of simplicial complex reduces to simplicial homology when N is taken to 2. We will begin with a brief review of simplicial complexes, the classical homology of simplicial complexes, and then generalize the discussion to Mayer homology.

Simplicial complex is a well-known topological model in data science, with notable examples including the Vietoris-Rips complex, Čech complex, and Alpha complex. A simplicial complex is composed of a collection of simplices following specific combinatorial rules. An n -simplex is the convex hull formed by n geometrically independent points. For example, a 0-simplex is a vertex, a 1-simplex is an edge, a 2-simplex is a triangle (with a solid interior), and a 3-simplex is a solid tetrahedron, as illustrated in Figure 1b.

Let $K = \{K_n\}$ be a simplicial complex, where K_n is the set of n -simplices. For a given field \mathbb{F} , we denote by $C_n(K)$ the \mathbb{F} -vector space generated by the n -simplices in K_n . The collection of

such groups $(C_n(K))_{n \geq 0}$ gives rise to a chain complex, with the differential defined by

$$d_n \langle v_0, v_1, \dots, v_n \rangle = \sum_{i=0}^n (-1)^i \langle v_0, \dots, \hat{v}_i, \dots, v_n \rangle,$$

where $\langle v_0, v_1, \dots, v_n \rangle$ is an n -simplex, and \hat{v}_i denotes the omission of the i -th vertex. It can be verified that $d_{n-1} \circ d_n = 0$. Thus, we obtain a chain complex

$$\dots \xrightarrow{d_{n+2}} C_{n+1}(K) \xrightarrow{d_{n+1}} C_n(K) \xrightarrow{d_n} C_{n-1}(K) \xrightarrow{d_{n-1}} \dots \quad (1)$$

We denote $\ker d_n = \{x \in C_n(K) \mid d_n x = 0\}$ and $\text{im } d_n = \{d_n x \mid x \in C_n(K)\}$. Since $d_{n-1} \circ d_n = 0$, it follows that $\text{im } d_{n+1} \subseteq \ker d_n$. The homology of the simplicial complex K is then defined by

$$H_n(K) := \frac{\ker d_n}{\text{im } d_{n+1}}, \quad n \geq 0. \quad (2)$$

The rank of $H_n(K)$ is the Betti number β_n . Betti numbers are widely used topological invariants of simplicial complexes. The geometric interpretation of β_0 , β_1 , and β_2 corresponds to the number of connected components, loops, and cavities, respectively.

The key idea of persistent homology is to introduce multi-scale information, which is provided by the filtration of simplicial complexes. For a given point cloud data set, the most common filtration of simplicial complexes is the Vietoris-Rips (VR) complex, as illustrated in [Figure 1c](#). Topological features at different scales exhibit a certain kind of persistence, meaning that homology generators at smaller scales may persist as homology generators at larger scales, thereby giving rise to persistent homology generators. The scale at which a generator is born is referred to as its birth time, while the scale at which it disappears is known as its death time. The topological features of persistent homology are represented by bars that record the birth and death times of homology generators, as shown in [Figure 1d](#), corresponding to the barcode of the filtration of simplicial complexes in [Figure 1d](#).

Unlike classical homology theories, the Mayer homology theory explored in this study generalizes the calculation of Betti numbers by utilizing the differential $d^N = 0$ with an integer $N \geq 2$ on the N -chain complex (see [Methods](#)). This approach allows us to obtain a family of homology groups $H_{n,q}(K)$ for a simplicial complex, where n is the dimension and $1 \leq q \leq N - 1$ corresponds to the Mayer degree. The homology groups $H_{n,q}(K)$ are referred to as Mayer homology. The Betti numbers associated with Mayer homology are termed the *Mayer Betti numbers* of the simplicial complex, denoted by $\beta_{k,q}$. For $N = 2$, the Mayer degree q can only be $q = 1$, which means that for a fixed dimension n , there is only one homology group, which is consistent with the usual homology groups of a simplicial complex. For general N , Mayer homology reveals more information than classical homology, offering potentially valuable geometric and topological features for applications. Beyond contributing to a unified mathematical framework for homology theory, Mayer homology and the associated Betti numbers provide valuable tools for analyzing the topological space of a given data set.

The Betti numbers for each simplicial complex are recorded in the barcode diagram shown in [Figure 1d](#). For example, the number of red lines in [Figure 1d](#) at a filtration parameter of 2 corresponds to β_0 . The Betti number $\beta_n : [0, +\infty) \rightarrow \mathbb{N}$ can be regarded as a function with the filtration parameter as its variable. Such a function is referred to as a *Betti curve*. [Figure 1e](#) shows

the Betti curves for $N = 2$, with the red line representing the Betti curve β_0 and the blue line representing the Betti curve β_1 . Additionally, Figure 1f and Figure 1g present the Betti curves for Mayer homology with $N = 3$ and $N = 5$, respectively. Each plot contains multiple curves because, in the case of Mayer homology, $\beta_{n,q}$ forms a curve for each $1 \leq q \leq N - 1$. It is worth noting that when $N = 5$, the $\beta_{k,2}$ and $\beta_{k,3}$ align with each other as shown in Figure 1f. The comparison of these figures highlights the richer topological and geometric features of Mayer Betti numbers. More detailed concepts and theorems associated with Mayer homology can be found in the Methods.

2.2 PMH-based element interactive molecular representation

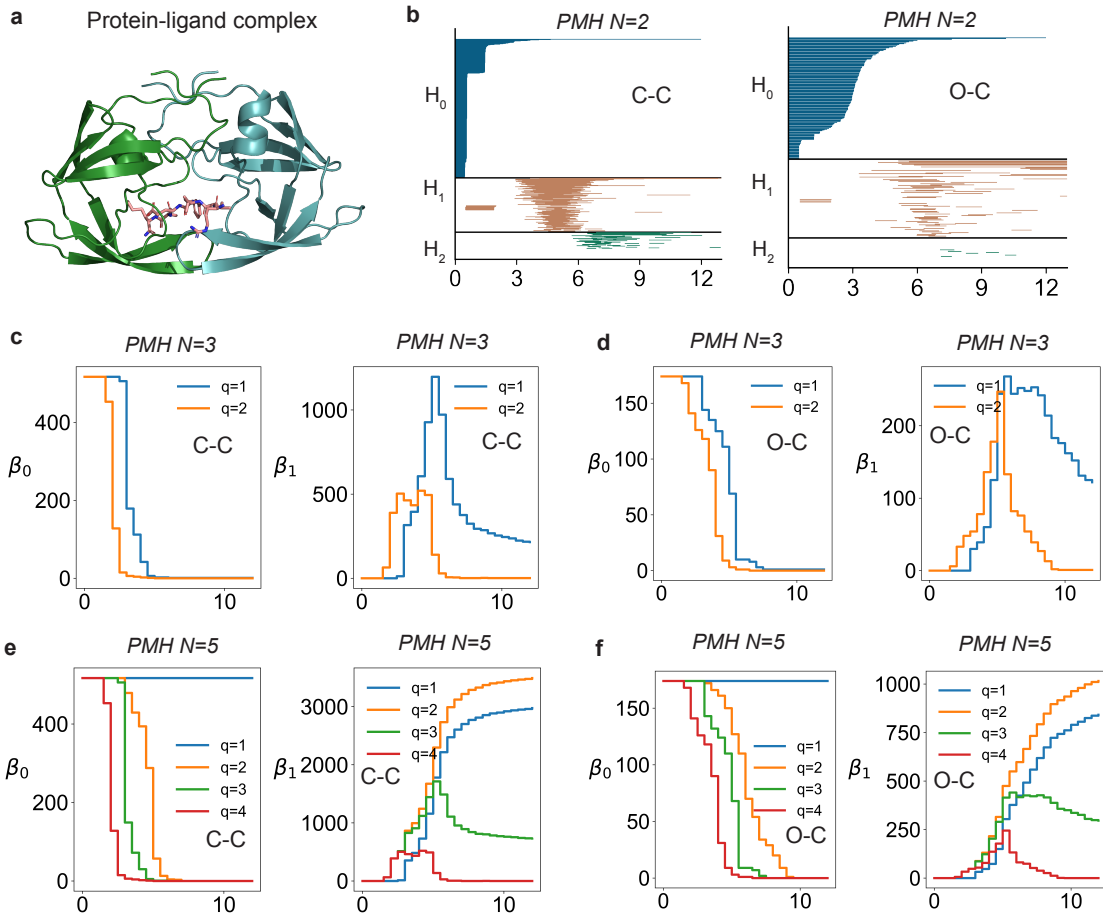


Figure 2: Persistent Mayer homology characterization for a protein-ligand complex (PDBID: 1A94) on alpha complex. **a:** The 3D structure of protein 1A94. The barcodes of different dimensions for a pair of atom sets in protein 1A94 with PMH ($N=2$). The first letter in C-C or O-C stands from atom group from protein and the second one indicates atom group from the ligand. **c-d:** The β_0^q and β_1^q calculations for the atom groups in **b** using PMH with $N=3$ and $q=1,2,\dots,N-1$. **e-f:** The β_0^q and β_1^q calculations for the atom groups in **b** using PMH with $N=5$ and $q=1,2,\dots,N-1$.

Atomic coordinates in molecules can be viewed as point cloud data. Persistent Mayer homology is well-suited for characterizing molecular structures, and a multiscale topological representation can be obtained through a filtration process. The resulting persistent features effectively capture the hierarchical and multiscale properties of biomolecular structures and interactions. Various in-

tramolecular and intermolecular interactions exist within molecular structures, characterized by different forces such as covalent bonds, van der Waals forces, electrostatic interactions, hydrophobic interactions, and hydrophilic interactions. To this end, we follow the element interaction characterization for pairwise atom groups [37] and use persistent Mayer homology to analyze these element-specific topological data structures. A cutoff distance of 12 Å is applied to extract the protein atoms around the ligand, considering that intermolecular interactions predominantly occur in the binding pocket region.

Figure 2b displays the PMH ($N = 2$) barcodes for C-C and O-C atom groups in the protein-ligand complex (PDBID: 1A94), with the simplicial complex constructed using the alpha complex. The persistence and variance of the β_0 , β_1 , and β_2 information are revealed. The ligand has more carbon atoms than oxygen atoms, leading to the faster decay of the β_0 value during filtration for C-C atom groups. Persistent attributes associated with β_1 and β_2 are also distinguishable in the characterization of C-C and O-C atom groups. The changes in $\beta_{k,q}$ values from PMH with $N = 3$ and $N = 5$ for C-C groups are shown in Figure 2c and Figure 2e. The changes for O-C groups are exhibited in Figure 2d and Figure 2f. Unlike the PMH characterization for 2D point clouds, which shows overlapping curves, there are distinct $\beta_{0,q}$ or $\beta_{1,q}$ curves in Figure 2d and Figure 2f for $N = 5$. These PMH ($N = 3$ or $N = 5$) Betti changes for these atom groups tend to plateau when the filtration parameter reaches 10 Å, or even as early as 5 Å. Therefore, it is sufficient to collect the Betti information with the filtration parameter ranging from 0 Å to 10 Å. For PMH ($N = 2$) or traditional persistent homology characterization of the protein-ligand complex, persistent attributes analysis extends to an upper filtration parameter of 12 Å.

It is observed that the $\beta_{0,1}$ and $\beta_{0,2}$ curves in Figure 2c resemble the $\beta_{0,3}$ and $\beta_{0,4}$ curves in Figure 2e. A similar pattern is seen between Figure 2d and Figure 2f. However, there are subtle numerical differences along the filtration. The $\beta_{0,1}$ and $\beta_{0,2}$ curves, along with the distinct $\beta_{1,q}$ curves, still differentiate PMH ($N = 5$) from PMH ($N = 3$).

A multiscale molecular representation can be obtained either by directly using PMH Betti numbers or by extracting useful statistical information from barcodes. Persistence bars represent the persistence of topological invariants in nested simplicial complexes, from which PMH Betti numbers can be directly read. Molecular features can be designed by collecting the Betti numbers at a set of filtration parameters. However, the inconsistent number of atoms across atom groups or molecules makes barcodes not directly suitable for scalable representation learning. Various stable learning strategies for topological data analysis have been proposed, such as persistent landscapes [38] and persistent images [39]. The bin-spaced statistical functions [18], incorporating the maximum, minimum, average, and standard deviation of barcodes, provide a reliable and effective vector representation. This approach offers competitive descriptive capacity and the advantage of scalable modeling. We utilize both the Betti numbers from PMH and barcodes to design molecular features.

To address computational efficiency, simplicial complexes using alpha complexes are primarily considered for PMH with $N > 2$. For PMH with $N = 2$, both VR complexes and alpha complexes can be utilized. When VR complexes are used, we incorporate physical properties in addition to the original molecular structure data to ensure that sufficient molecular interactions are captured. Technically, the filtration process and persistent Mayer homology are induced using either the Euclidean distance metric in space or a kernel function-defined correlation matrix for a group of atomic

coordinates. Collectively, these methods enhance our PMH theory-based molecular representation learning. We provide more details about our PMH features in the following section.

2.3 PMH learning models for drug design

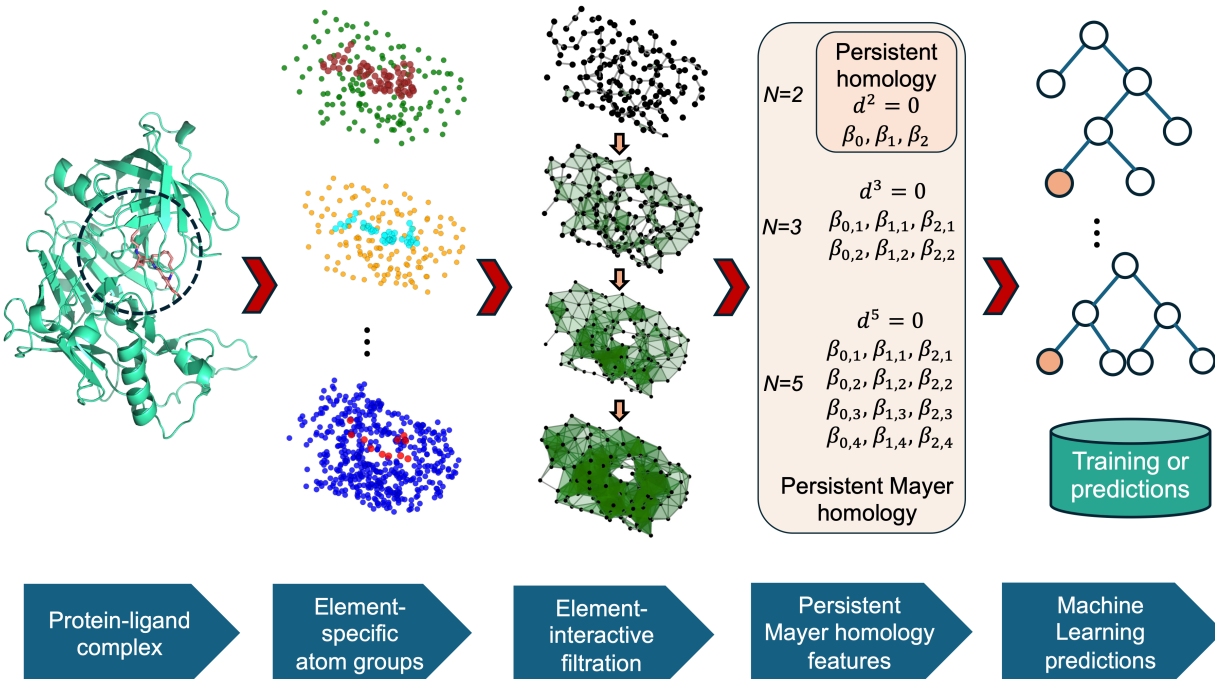


Figure 3: The illustration of persistent Mayer homology feature extraction for a protein-ligand complex (PDBID: 1A94) and the subsequent machine learning model development.

2.3.1 PMH-based multiscale molecular vectorization

We utilize element-interactive PMH representation learning for biomolecular data, as discussed above. This strategy captures crucial biological information and enhances characterization capacity, as validated by extensive modeling work [18, 40, 29]. Specifically, for a protein-ligand complex, the types of elements considered for proteins are $S_P = \{C, N, O, S\}$, and for ligands, they are $S_L = \{C, N, O, S, P, F, Cl, Br, I\}$. Therefore, we can have up to 36 element combinations and design interactive PMH features accordingly. The interactions between all the ligand atoms and protein atoms near the binding pocket can also be characterized by PMH.

We denote S_{X-Y}^c as the set of atoms consisting of X types of atoms in the protein and Y types of atoms in the ligand, where the distance between any pair of atoms in these two groups is within a cutoff c :

$$S_{X-Y}^c = \{a|a \in X, \min_{b \in Y} \text{dis}(a, b) \leq c\} \cup \{b|b \in Y\}, \quad (3)$$

where a and b denote atoms. We also consider all heavy atoms in the ligand together with all heavy atoms in the protein that are within the cutoff distance c from the ligand molecule, and denote this

set as S_{all}^c . Similarly, we denote the set of all heavy atoms in the protein that are within the cutoff distance c from the ligand molecule as S_{pro}^c .

Both the correlation matrix and the Euclidean distance matrix are used for the VR complex-induced persistent homology (PMH) ($N = 2$). We use $A(i)$ to indicate the affiliation of an atom with index i in a group of atoms from either the protein or the ligand. We define four types of matrices as follows.

- $FRI_{\tau,\nu}^{agst}$:

$$d(i, j) = \begin{cases} 1 - e^{-(r_{ij}/\eta_{ij})^\kappa}, & A(i) \neq A(j) \\ d_\infty, & A(i) = A(j) \end{cases} \quad (4)$$

- $FRI_{\tau,\nu}$:

$$d(i, j) = 1 - e^{-(r_{ij}/\eta_{ij})^\kappa} \quad (5)$$

- EUC^{agst} :

$$d(i, j) = \begin{cases} r_{ij}, & A(i) \neq A(j) \\ d_\infty, & A(i) = A(j) \end{cases} \quad (6)$$

- EUC :

$$d(i, j) = r_{ij}. \quad (7)$$

[Equation 4](#) is inspired by the development of the flexibility-rigidity index (FRI) theory [\[41\]](#), which utilizes a decaying radial basis function to effectively quantify atomic interactions. The parameter r_{ij} represents the Euclidean distance between atoms with indices i and j , and $\eta_{ij} = \tau \cdot (r_i + r_j)$, where k and τ are positive adjustable parameters that control the decay rate of the exponential kernel, allowing us to model interactions with different strengths. Here, η_{ij} is the characteristic distance between the i th and j th atoms and is typically set as the sum of the van der Waals radii of the two atoms. The exponential kernel function is non-negative and strictly monotonically decreasing with respect to the Euclidean distance between a pair of atoms. When the Euclidean distance between two atoms is close to 0, their correlation distance $d(i, j)$ approaches 1. Conversely, when the atoms are far apart, $d(i, j)$ approaches 0. This ensures that the correlation matrix is well-defined. We use the superscript *agst* to distinguish correlations between atoms from the same or different affiliations. When both atoms are within the same molecule, their correlation distance is set to infinity. This approach excludes intramolecular interactions and highlights the intermolecular interactions between proteins and ligands, which are then represented in the construction of VR simplices and ultimately aid in characterizing these interactions through persistent Mayer homology (PMH).

In contrast, the correlation matrix defined by [Equation 5](#) captures both physical and chemical information from intramolecular and intermolecular interactions. Furthermore, [Equation 6](#) and [Equation 7](#), which are based on the Euclidean distance metric, provide a better characterization of molecular 3D structures. The EUC^{agst} metric places greater emphasis on the shape derived from intermolecular 3D data and is used in conjunction with alpha complexes for our PMH analysis. We primarily use PMH($N=2$) and PMH($N=5$) to extract molecular features, employing five different feature extraction strategies as shown in [Table 1](#). Consequently, for each protein-ligand complex, we generate five feature vectors: the first four are derived from PMH($N=2$), while the final vector is based on PMH($N=5$).

I	PMH2($P_{\text{ep-el}}^{12}$, FRI ^{agst} , VR) ep $\in S_P$, el $\in S_L$	Length sum of all Betti-0 bars.
II	PMH2(P_{all}^6 , FRI, VR) PMH2(P_{pro}^6 , FRI, VR)	Length sum and birth sum of Betti-0, Betti-1, and Betti-2 bars for protein, complex, as well as the sum differences between protein and complex.
III	PMH2($P_{\text{ep-el}}^{12}$, EUC ^{agst} , VR) ep $\in S_P$, el $\in S_L$	Counts of Betti-0 bars with ‘death’ values within each interval: [0, 2.5], [2.5, 3], [3, 3.5], [3.5, 4.5], [4.5, 6], [6, 12].
IV	PMH2(P_{all}^9 , EUC, Alpha) PMH2(P_{pro}^9 , EUC, Alpha)	Length sum of Betti-1 and Betti-2 bars with ‘birth’ values within each interval: [0, 2], [2, 3], [3, 4], [4, 5], [5, 6], [6, 9]. The sum differences between complex and protein are also considered.
V	PMH5($P_{\text{ep-el}}^{12}$, EUC, Alpha) ep $\in S_P \setminus \{C\}$, el $\in S_L \cup \{H\}$ ep $\in \{C\}$, el $\in S_L \cup \{H\}$	$\beta_{k,q}$ (k=0,1, q=1,2,...,4) over filtration parameter range from 0 to 10 with stepsize of 0.2. $\beta_{k,q}$ (k=0,1, q=1,2,...,4) over filtration parameter range from 0 to 8 with stepsize of 0.5.

Table 1: Molecular feature extraction with PMH. PMH2 and PMH5 indicates the PMH on 2-chain and 5-chain complex, respectively. The first argument in PMH2 or PMH5 specifies the group of molecular coordinate data, while the second argument denotes the correlation or Euclidean distance matrix. The third argument indicates the type of complex used to construct simplicial complex.

2.3.2 PMH learning models for binding affinity prediction

We demonstrate the learning capacity of the proposed PMH through protein-ligand binding affinity prediction, a critical problem in drug discovery. We consider three well-established PDBbind datasets [36], including PDBbind-v2007, PDBbind-v2013, and PDBbind-v2016. These datasets contain a collection of 3D structures for protein-ligand complexes and their experimental binding affinities and have been widely used to test new methods [42, 43, 44]. Detailed information about the data size for the three datasets and the related training-test splits can be found in Table 2. Based on the 3D structures, each protein-ligand complex is represented by five sets of molecular vectors according to Table 1. In our implementation, feature sets I-IV are concatenated into a long vector representation, while feature set V is used as a separate vector representation. These two vectors are combined with the gradient boosting decision tree (GBDT) algorithm to build regression models, resulting in model-PMH2 and model-PMH5. The GBDT hyperparameters used for modeling are listed in Table 3. A general workflow of our PMH featurization and the resulting machine learning modeling is provided in Figure 3.

The final PMH modeling prediction is determined by the consensus of the predictions from the two models. We build models twenty times with different random seeds and use two evaluation metrics: Pearson correlation coefficient (R) and root mean square error (RMSE). The average R values of the PMH machine learning models for the three datasets are 0.824, 0.787, and 0.834, respectively, as shown in Table 4. These high R values validate the effectiveness and reliability of our PMH molecular representation. We also obtain low RMSE values (in units of kcal/mol), which compare the predicted binding energies with the experimental values. The binding energy is

calculated from the given pK_d in the original data by multiplying it by a constant of 1.3633.

To enhance the predictive performance of our PMH machine learning models, we incorporate natural language processing (NLP)-based molecular features and develop an additional set of machine learning models. The pretrained NLP models generate molecular features using molecular sequences as input. Specifically, we utilize molecular features from transformer-based pretrained models for proteins [45] and small molecules [11]. These features are then integrated with the GBDT algorithm to create a new predictive model, referred to as model-seq. The modeling performance of this approach is presented in the third column of Table 4. The average R value of the PMH model exceeds that of the transformer-based machine learning model. Additionally, we create a consensus model by combining the strengths of the three models—model-PMH2, model-PMH5, and model-seq—by averaging their predictions to determine the final predicted binding affinity. The last column of Table 4 shows the performance of the consensus model. The consensus model significantly boosts the performance of the PMH model, with an average R value of 0.832.

A series of advanced mathematical theories from algebraic topology and graph theory were employed to design molecular descriptors [40, 29, 46, 18], leading to reliable machine learning models. Their success significantly relies on molecular characterization through topological invariants. Our machine learning model is comparable to these competitive models and demonstrates superior performance compared to a wide range of other published models. The Betti numbers from PMH include crucial topological invariants and provide additional mathematical analysis of molecular data. This significantly enhances the descriptive and predictive power of our molecular features.

Dataset	Total	Training set	Test set
PDBbind-v2007 [47]	1300	1105	195
PDBbind-v2013 [48]	2959	2764	195
PDBbind-v2016 [49]	4057	3767	290

Table 2: Details of the datasets utilized for benchmark tests in this study.

No. of estimators	Max depth	Min. sample split	Learning rate
20000	7	5	0.002
Max features	Subsample size	Repetition	
Square root	0.8	20 times	

Table 3: Hyperparameters used for build gradient boosting regression models.

Dataset	PMH	Transformer	PMH+Transformer
PDBbind-v2007	0.824(1.95)	0.795(2.006)	0.837(1.907)
PDBbind-v2013	0.787(2.036)	0.791(1.977)	0.807(1.982)
PDBbind-v2016	0.834(1.755)	0.836(1.716)	0.851(1.701)
Average	0.815 (1.914)	0.807 (1.9)	0.832 (1.863)

Table 4: Modeling performance of different strategies on the test sets of PDBbind-v2007, PDBbind-v2013 and PDBbind-v2016. Pearson correlation coefficient and root mean square error (unit, kcal/mol) are the two evaluation metrics.

We compare the performance of our consensus model with various models from the literature.

Figure 4 depicts these comparisons across the three PDBbind datasets. Our model outperforms a wide range of models and represents the state of the art. The second column in Figure 4 shows the comparison between experimental energy and predictions from our final consensus model. The high consistency between the two sets of binding energies validates the accuracy and reliability of our machine learning model. Deep neural networks have advanced the development of the scientific community. Integrating our PMH molecular descriptors with deep neural networks has the potential to offer even more accurate predictive models.

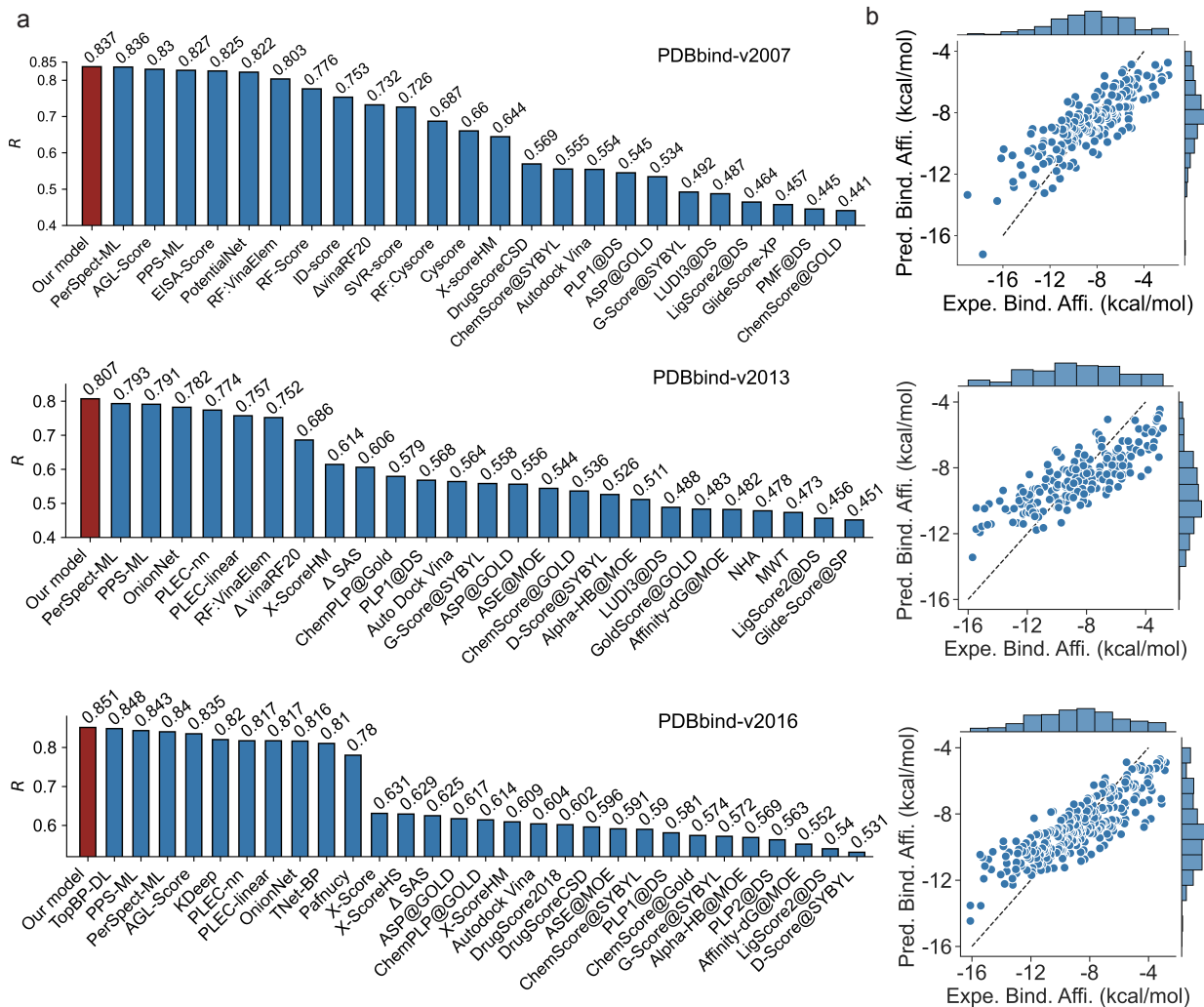


Figure 4: The prediction performance of my final machine learning model for three well-established protein-ligand binding affinity datasets including PDBbind-v2007, PDBbind-v2013, and PDBbind-v2016. The comparison of the experimental and predicted binding affinities for the three datasets are exhibited in the right column.

3 Discussion

Molecular feature extraction plays a fundamental role in AI-driven drug design. End-to-end molecular representation learning using deep neural networks, such as CNNs and GNNs [15, 16, 50],

has been developed and shown impressive capabilities in analyzing biological data and predicting protein-ligand binding affinities. In contrast, molecular featurization or engineering takes a different approach by encoding the structural, physical, chemical, or biological properties of molecules. Among the various molecular featurization methods, those based on advanced mathematics have emerged as a highly promising strategy for significantly enhancing molecular featurization capabilities.

Geometric, topological, and combinatorial invariants from differential geometry, algebraic topology, and algebraic graph theory have proven to be valuable mathematical techniques in this regard [40, 26, 29, 46, 18]. These mathematical molecular representations are characterized by a higher level of abstraction and transferability. Persistent homology has demonstrated high effectiveness for molecular featurization by employing topological invariants and their persistence along a filtration process. The proposed persistent Mayer homology theory extends persistent homology while preserving its power. Specifically, the Betti number information derived from Mayer homology theory across different N -chain complexes includes the Betti number information of the usual simplicial homology when N is reduced to 2. The utilization of filtration induces multiscale representations by collecting sufficient Betti number information from persistent Mayer homology. The molecular features induced by PMH can further enhance the descriptive and predictive capacity of the original persistent homology theory and lead to learning models with boosted performance.

We primarily focus on PMH5 for simplicial complexes derived from Alpha complexes due to concerns about computation time and cost. To enhance efficiency, particularly when dealing with VR complexes, more efficient computer programs can be developed. Recently, a series of topological persistent Laplacian theories have been proposed [29, 46, 28] and applied to the design of molecular features. The harmonic spectral information of these Laplacians recovers the Betti numbers of persistent homology, while the non-harmonic spectral information provides additional geometric insights into the data. Additionally, a Persistent Mayer Laplacian based on simplicial complexes was developed in our recent study [35]. We will further explore the potential of Persistent Mayer Laplacian for molecular representation learning in our future work. Other significant advancements in molecular featurization include the application of persistent de Rham-Hodge Laplacians [32]. These methods demonstrate competitive performance and high potential. One key difference between these approaches and persistent homology or persistent Mayer homology is that they utilize curve-shaped data or continuum manifolds, whereas persistent homology and persistent Mayer homology focus on point cloud data. Our work in persistent Mayer homology advances the development of persistent homology and maintains its competitiveness.

4 Methods

4.1 Persistent Mayer homology theory

In this section, we introduce the mathematical theory of Persistent Mayer Homology (PMH). PMH builds on several key mathematical concepts, including N -chain complexes, Mayer homology, and Mayer Betti numbers. Persistent homology, a crucial theory in algebraic topology, serves as the foundation for PMH. However, PMH extends persistent homology by providing a broader mathematical framework that includes higher-order analysis.

N -chain complex and generalized differential. Let \mathbb{C} be the field of complex numbers, an N -

chain complex is constructed as a graded \mathbb{C} -linear space $C_* = (C_n)_{n \geq 0}$, equipped with linear maps $d_n : C_n \rightarrow C_{n-1}$ of degree -1 . A key property of these differentials d_n is that when applied N times, they vanish, meaning $d^N = 0$. This property is fundamental to the structure of the N -chain complex and allows for the development of a homological theory based on these complexes.

Suppose K is a simplicial complex. The generalized differential of the simplicial complex is defined on the graded space $C_* = (C_n)_{n \geq 0}$, where C_n is generated by the n -simplices of K . The differential d_n acts on an n -simplex $\langle v_0, v_1, \dots, v_n \rangle$ by summing over the contributions of the $(n-1)$ -simplices obtained by omitting one vertex at a time:

$$d_n \langle v_0, v_1, \dots, v_n \rangle = \sum_{i=0}^n \xi^i \langle v_0, \dots, \hat{v}_i, \dots, v_n \rangle,$$

where ξ is the N -th primitive root of unity, and \hat{v}_i denotes the omission of the i -th vertex. This differential satisfies the property $d^N = 0$, a result stemming from the cyclic nature of the root of unity ξ .

Mayer Homology. Given a simplicial complex K , we can obtain the N -chain complex and generalized differential (C_*, d) . For an integer q such that $1 \leq q \leq N-1$, we have the following:

$$C_{n+N-q} \xrightarrow{d^{N-q}} C_n \xrightarrow{d^q} C_{n-q}.$$

Note that $d^q \circ d^{N-q} = d^N = 0$, the above is a classical chain complex. In general, we have

$$\begin{array}{ccccccccccc} \cdots & \xrightarrow{d} & C_{n+N-1} & \xrightarrow{d^{N-1}} & C_n & \xrightarrow{d} & C_{n-1} & \xrightarrow{d^{N-1}} & C_{n-N} & \xrightarrow{d} & C_{n-N-1} & \longrightarrow \cdots \\ & & \downarrow d & & \downarrow id & & \downarrow d & & \downarrow id & & \downarrow d & \\ \cdots & \xrightarrow{d^2} & C_{n+N-2} & \xrightarrow{d^{N-2}} & C_n & \xrightarrow{d^2} & C_{n-2} & \xrightarrow{d^{N-2}} & C_{n-N} & \xrightarrow{d^2} & C_{n-N-2} & \longrightarrow \cdots \\ & & \downarrow d & & \downarrow id & & \downarrow d & & \downarrow id & & \downarrow d & \\ \vdots & & \vdots & & \vdots & & \vdots & & \vdots & & \vdots & \\ & & \downarrow d & & \downarrow id & & \downarrow d & & \downarrow id & & \downarrow d & \\ \cdots & \xrightarrow{d^{N-2}} & C_{n+2} & \xrightarrow{d^2} & C_n & \xrightarrow{d^{N-2}} & C_{n-N+2} & \xrightarrow{d^2} & C_{n-N} & \xrightarrow{d^{N-2}} & C_{n-2N+2} & \longrightarrow \cdots \\ & & \downarrow d & & \downarrow id & & \downarrow d & & \downarrow id & & \downarrow d & \\ \cdots & \xrightarrow{d^{N-1}} & C_{n+1} & \xrightarrow{d} & C_n & \xrightarrow{d^{N-1}} & C_{n-N+1} & \xrightarrow{d} & C_{n-N} & \xrightarrow{d^{N-1}} & C_{n-2N+1} & \longrightarrow \cdots \end{array}$$

Thus we could give the (n, q) -th Mayer homology group of simplicial complex K :

$$H_{n,q}(K) = H_{n,q}(C_*, d) = \frac{\ker d^q}{\text{im } d^{N-q}} = \frac{\{x \in C_n \mid d^q x = 0\}}{\{d^{N-q} y \mid y \in C_{n+N-q}\}}.$$

The rank of $H_{n,q}(K)$ is defined to be the Mayer Betti number, denoted as $\beta_{n,q}$. Specifically, $\beta_{n,q}$ is defined as the dimension of the vector space $H_{n,q}(K)$:

$$\beta_{n,q} = \dim H_{n,q}(K).$$

These numbers provide a quantitative measure of the topological and geometric complexity of the complex in the context of Mayer homology.

Persistent Mayer homology. We will study the persistence of these topological features across different scales based on the filtration of simplicial complexes. For a non-decreasing real-valued function $f : K \rightarrow \mathbb{R}$, we can obtain a filtration of simplicial complexes

$$K_{a_1} \subseteq K_{a_2} \subseteq \cdots \subseteq K_{a_m} = K,$$

for $a_1 \leq a_2 \leq \cdots \leq a_m$. Here,

$$K_a = \{\sigma \in K \mid f(\sigma) \leq a\}.$$

As the filtration parameter a increases, the simplicial complex K_a grows, allowing for the analysis of how features of Mayer homology evolve.

Persistent Mayer homology is defined by examining the Mayer homology groups at different stages of the filtration. The persistent Mayer homology groups $H_{n,q}^{a,b}$ measure the topological and geometric features that persist from the simplicial complex K_a to K_b . Specifically, these groups are defined as:

$$H_{n,q}^{a,b} = \text{im} (H_{n,q}(K_a) \rightarrow H_{n,q}(K_b)), \quad a \leq b.$$

These persistent features can be visualized using persistence diagrams or barcodes, offering insights into the multi-scale topological and geometric structure of the data.

4.2 Natural language processing (NLP) molecular descriptors

We incorporate molecular descriptors derived from natural language processing (NLP) techniques to improve the performance of PMH machine learning models. A protein-ligand complex comprises the 3D structures of both the protein and the ligand. For these structures, sequence representations are utilized: amino acid sequences for the protein and SMILES strings for the ligand. NLP techniques are applied to design molecular features for each component. We then concatenate the molecular features from both parts into a single feature vector, which serves as the molecular descriptor for the entire protein-ligand complex.

4.2.1 ESM transformer protein language model

In recent years, significant progress has been made in modeling protein properties using large-scale protein transformer models trained on extensive datasets of protein sequences. A notable example is the ESM-2 transformer protein language model introduced by Rives et al. [45], which extracts underlying biological properties and relationships by deeply analyzing vast quantities of amino acids protein sequences. This model was trained on a dataset consisting of 250 million sequences using a masked filling procedure and features a sophisticated architecture with 34 layers and an impressive 650 million parameters.

We utilized the ESM transformer model to generate sequence embeddings for the protein part. At each layer of the ESM model, a sequence of length L is encoded into a matrix of size $1280 \times L$, excluding the start and terminal tokens. For our machine learning predictions, we used the sequence representation from the final (34th) layer and computed the average along the sequence length axis, resulting in a 1280-component vector.

4.2.2 Transformer-based small molecular language model

A transformer-based deep learning model was proposed to extract molecular representations [13] and is a valuable tool for small molecule machine learning analysis [51, 52]. This model was trained on over 700 million SMILES strings sourced from databases such as ChEMBL, PubChem, and ZINC. Three pretrained models were developed: model-C, model-CP, and model-CPZ. For each molecule, the model generates a 256×512 dimensional matrix, where 256 represents the symbols associated with the molecule, and 512 denotes the vector dimension for each symbol. The molecular features are given by the average of the 256 vectors.

Funding Information

This work was supported in part by NIH grants R01GM126189, R01AI164266, and R35GM148196, NSF grants DMS-2052983, DMS-1761320, DMS-2245903, and IIS-1900473, NASA grant 80NSSC21M0023, MSU Foundation, Bristol-Myers Squibb 65109, and Pfizer.

Statement of Usage of Artificial Intelligence

In the preparation of this manuscript, we utilized ChatGPT primarily to assist with improving the clarity and grammar of the English text. The AI tool was employed solely for language enhancement and did not contribute to the research content or data analysis.

Data Availability

All data and the code needed to reproduce this paper’s result can be found at https://github.com/WeilabMSU/PMH_Bio.

Author Contributions

Hongsong Feng was responsible for the coding, computational experiments and writing. Li Shen was responsible for the coding and some writing. Jian Liu was responsible for the coding and some writing. Guo-Wei Wei was responsible for methodology, reviewing, editing, some writing and supervision.

Conflict of Interest

The authors declare no conflict of interest.

ORCID

Hongsong Feng- <https://orcid.org/0000-0001-8039-3059>

Li Shen - <https://orcid.org/0009-0003-0318-8328>

Jian Liu - <https://orcid.org/0000-0003-4362-5273>

Data and code availability

All data and the code needed to reproduce this paper’s result can be found at https://github.com/WeilabMSU/PMH_Bio.

Acknowledgment

This work was supported in part by NIH grants R01GM126189, R01AI164266, and R35GM148196, NSF grants DMS-2052983, DMS-1761320, DMS-2245903, and IIS-1900473, NASA grant 80NSSC21M0023, MSU Foundation, Bristol-Myers Squibb 65109, and Pfizer.

References

- [1] Nic Fleming. Computer-calculated compounds. *Nature*, 557(7707):S55–7, 2018.
- [2] Hongjian Li, Kwong-Sak Leung, Man-Hon Wong, and Pedro J Ballester. Improving autodock vina using random forest: the growing accuracy of binding affinity prediction by the effective exploitation of larger data sets. *Molecular informatics*, 34(2-3):115–126, 2015.
- [3] Evan N Feinberg, Debnil Sur, Zhenqin Wu, Brooke E Husic, Huanghao Mai, Yang Li, Saisai Sun, Jianyi Yang, Bharath Ramsundar, and Vijay S Pande. Potentialnet for molecular property prediction. *ACS central science*, 4(11):1520–1530, 2018.
- [4] Pedro J Ballester and John BO Mitchell. A machine learning approach to predicting protein–ligand binding affinity with applications to molecular docking. *Bioinformatics*, 26(9):1169–1175, 2010.
- [5] Xiaolin Pan, Hao Wang, Yueqing Zhang, Xingyu Wang, Cuiyu Li, Changge Ji, and John ZH Zhang. Aa-score: a new scoring function based on amino acid-specific interaction for molecular docking. *Journal of Chemical Information and Modeling*, 62(10):2499–2509, 2022.
- [6] Cheng Wang and Yingkai Zhang. Improving scoring-docking-screening powers of protein–ligand scoring functions using random forest. *Journal of computational chemistry*, 38(3):169–177, 2017.
- [7] Shukai Gu, Chao Shen, Jiahui Yu, Hong Zhao, Huanxiang Liu, Liwei Liu, Rong Sheng, Lei Xu, Zhe Wang, Tingjun Hou, et al. Can molecular dynamics simulations improve predictions of protein-ligand binding affinity with machine learning? *Briefings in bioinformatics*, 24(2):bbad008, 2023.
- [8] Thereza A Soares, Ariane Nunes-Alves, Angelica Mazzolari, Fiorella Ruggiu, Guo-Wei Wei, and Kenneth Merz. The (re)-evolution of quantitative structure–activity relationship (qsar)

- studies propelled by the surge of machine learning methods. *Journal of Chemical Information and Modeling*, 62(22):5317–5320, 2022.
- [9] Akinori Sato, Tomoyuki Miyao, Swarit Jasial, and Kimito Funatsu. Comparing predictive ability of qsar/qspr models using 2d and 3d molecular representations. *Journal of Computer-Aided Molecular Design*, 35:179–193, 2021.
 - [10] Joseph L Durant, Burton A Leland, Douglas R Henry, and James G Nourse. Reoptimization of mdl keys for use in drug discovery. *Journal of chemical information and computer sciences*, 42(6):1273–1280, 2002.
 - [11] Robin Winter, Floriane Montanari, Frank Noé, and Djork-Arné Clevert. Learning continuous and data-driven molecular descriptors by translating equivalent chemical representations. *Chemical science*, 10(6):1692–1701, 2019.
 - [12] Roberto Todeschini and Viviana Consonni. *Handbook of molecular descriptors*. John Wiley & Sons, 2008.
 - [13] Dong Chen, Jiaxin Zheng, Guo-Wei Wei, and Feng Pan. Extracting predictive representations from hundreds of millions of molecules. *The journal of physical chemistry letters*, 12(44):10793–10801, 2021.
 - [14] Thin Nguyen, Hang Le, Thomas P Quinn, Tri Nguyen, Thuc Duy Le, and Svetha Venkatesh. Graphdta: predicting drug–target binding affinity with graph neural networks. *Bioinformatics*, 37(8):1140–1147, 2021.
 - [15] Izhar Wallach, Michael Dzamba, and Abraham Heifets. Atomnet: a deep convolutional neural network for bioactivity prediction in structure-based drug discovery. *arXiv preprint [arXiv:1510.02855](https://arxiv.org/abs/1510.02855)*, 2015.
 - [16] Matthew Ragoza, Joshua Hochuli, Elisa Idrobo, Jocelyn Sunseri, and David Ryan Koes. Protein–ligand scoring with convolutional neural networks. *Journal of chemical information and modeling*, 57(4):942–957, 2017.
 - [17] José Jiménez, Miha Skalic, Gerard Martinez-Rosell, and Gianni De Fabritiis. K deep: protein–ligand absolute binding affinity prediction via 3d-convolutional neural networks. *Journal of chemical information and modeling*, 58(2):287–296, 2018.
 - [18] Zixuan Cang and Guo-Wei Wei. Topologynet: Topology based deep convolutional and multi-task neural networks for biomolecular property predictions. *PLoS computational biology*, 13(7):e1005690, 2017.
 - [19] Wanying Bi, Xin Fu, Jingyan Li, and Jie Wu. Persistent magnitude for the quantitative analysis of the structure and stability of carboranes. *J. Comput. Biophys. Chem*, 1(11):11, 2024.
 - [20] Gunnar Carlsson and Afra Zomorodian. The theory of multidimensional persistence. In *Proceedings of the twenty-third annual symposium on Computational geometry*, pages 184–193, 2007.

- [21] Herbert Edelsbrunner, John Harer, et al. Persistent homology-a survey. *Contemporary mathematics*, 453(26):257–282, 2008.
- [22] Afra Zomorodian and Gunnar Carlsson. Computing persistent homology. In *Proceedings of the twentieth annual symposium on Computational geometry*, pages 347–356, 2004.
- [23] Gunnar Carlsson and Vin De Silva. Zigzag persistence. *Foundations of computational mathematics*, 10:367–405, 2010.
- [24] Menglun Wang, Zixuan Cang, and Guo-Wei Wei. A topology-based network tree for the prediction of protein–protein binding affinity changes following mutation. *Nature Machine Intelligence*, 2(2):116–123, 2020.
- [25] Duc Duy Nguyen, Zixuan Cang, Kedi Wu, Menglun Wang, Yin Cao, and Guo-Wei Wei. Mathematical deep learning for pose and binding affinity prediction and ranking in d3r grand challenges. *Journal of computer-aided molecular design*, 33:71–82, 2019.
- [26] Duc Duy Nguyen, Zixuan Cang, and Guo-Wei Wei. A review of mathematical representations of biomolecular data. *Physical Chemistry Chemical Physics*, 22(8):4343–4367, 2020.
- [27] Jiahui Chen, Rui Wang, Menglun Wang, and Guo-Wei Wei. Mutations strengthened sars-cov-2 infectivity. *Journal of molecular biology*, 432(19):5212–5226, 2020.
- [28] Rui Wang, Duc Duy Nguyen, and Guo-Wei Wei. Persistent spectral graph. *International journal for numerical methods in biomedical engineering*, 36(9):e3376, 2020.
- [29] Zhenyu Meng and Keli Xia. Persistent spectral-based machine learning (perspect ml) for protein-ligand binding affinity prediction. *Science advances*, 7(19):eabc5329, 2021.
- [30] Xiaoqi Wei, Jiahui Chen, and Guo-Wei Wei. Persistent topological laplacian analysis of sars-cov-2 variants. *Journal of computational biophysics and chemistry*, 22(5):569, 2023.
- [31] Jiahui Chen, Yuchi Qiu, Rui Wang, and Guo-Wei Wei. Persistent laplacian projected omicron ba. 4 and ba. 5 to become new dominating variants. *Computers in Biology and Medicine*, 151:106262, 2022.
- [32] Zhe Su, Yiyong Tong, and Guo-Wei Wei. Persistent de rham-hodge laplacians in the eulerian representation. *arXiv preprint [arXiv:2408.00220](https://arxiv.org/abs/2408.00220)*, 2024.
- [33] Jian Liu, Dong Chen, Feng Pan, and Jie Wu. Neighborhood path complex for the quantitative analysis of the structure and stability of carboranes. *Journal of Computational Biophysics and Chemistry*, 22(04):503–511, 2023.
- [34] Walther Mayer. A new homology theory. *Annals of Mathematics*, pages 370–380, 1942.
- [35] Li Shen, Jian Liu, and Guo-Wei Wei. Persistent mayer homology and persistent mayer laplacian. *Foundations of Data Science*, pages 0–0, 2024.

- [36] Zhihai Liu, Yan Li, Li Han, Jie Li, Jie Liu, Zhixiong Zhao, Wei Nie, Yuchen Liu, and Renxiao Wang. Pdb-wide collection of binding data: current status of the pddbbind database. *Bioinformatics*, 31(3):405–412, 2015.
- [37] Zixuan Cang and Guo-Wei Wei. Integration of element specific persistent homology and machine learning for protein-ligand binding affinity prediction. *International journal for numerical methods in biomedical engineering*, 34(2):e2914, 2018.
- [38] Peter Bubenik et al. Statistical topological data analysis using persistence landscapes. *J. Mach. Learn. Res.*, 16(1):77–102, 2015.
- [39] Henry Adams, Tegan Emerson, Michael Kirby, Rachel Neville, Chris Peterson, Patrick Shipman, Sofya Chepushtanova, Eric Hanson, Francis Motta, and Lori Ziegelmeier. Persistence images: A stable vector representation of persistent homology. *Journal of Machine Learning Research*, 18(8):1–35, 2017.
- [40] Duc Duy Nguyen and Guo-Wei Wei. Agl-score: algebraic graph learning score for protein–ligand binding scoring, ranking, docking, and screening. *Journal of chemical information and modeling*, 59(7):3291–3304, 2019.
- [41] Kelin Xia, Kristopher Opron, and Guo-Wei Wei. Multiscale multiphysics and multidomain models—flexibility and rigidity. *The Journal of chemical physics*, 139(19):11B614.1, 2013.
- [42] Md Masud Rana and Duc Duy Nguyen. Geometric graph learning with extended atom-types features for protein-ligand binding affinity prediction. *Computers in Biology and Medicine*, 164:107250, 2023.
- [43] Md Masud Rana and Duc Duy Nguyen. Eisa-score: Element interactive surface area score for protein–ligand binding affinity prediction. *Journal of Chemical Information and Modeling*, 62(18):4329–4341, 2022.
- [44] Xiang Liu, Huitao Feng, Jie Wu, and Kelin Xia. Dowker complex based machine learning (dcml) models for protein-ligand binding affinity prediction. *PLoS computational biology*, 18(4):e1009943, 2022.
- [45] Alexander Rives, Joshua Meier, Tom Sercu, Siddharth Goyal, Zeming Lin, Jason Liu, Demi Guo, Myle Ott, C Lawrence Zitnick, Jerry Ma, et al. Biological structure and function emerge from scaling unsupervised learning to 250 million protein sequences. *Proceedings of the National Academy of Sciences*, 118(15):e2016239118, 2021.
- [46] Ran Liu, Xiang Liu, and Jie Wu. Persistent path-spectral (pps) based machine learning for protein–ligand binding affinity prediction. *Journal of Chemical Information and Modeling*, 63(3):1066–1075, 2023.
- [47] Tiejun Cheng, Xun Li, Yan Li, Zhihai Liu, and Renxiao Wang. Comparative assessment of scoring functions on a diverse test set. *Journal of chemical information and modeling*, 49(4):1079–1093, 2009.

- [48] Yan Li, Zhihai Liu, Jie Li, Li Han, Jie Liu, Zhixiong Zhao, and Renxiao Wang. Comparative assessment of scoring functions on an updated benchmark: 1. compilation of the test set. *Journal of chemical information and modeling*, 54(6):1700–1716, 2014.
- [49] Minyi Su, Qifan Yang, Yu Du, Guoqin Feng, Zhihai Liu, Yan Li, and Renxiao Wang. Comparative assessment of scoring functions: the casf-2016 update. *Journal of chemical information and modeling*, 59(2):895–913, 2018.
- [50] Hussein Hassan-Harrirou, Ce Zhang, and Thomas Lemmin. Rosenet: improving binding affinity prediction by leveraging molecular mechanics energies with an ensemble of 3d convolutional neural networks. *Journal of chemical information and modeling*, 60(6):2791–2802, 2020.
- [51] Nicole Hayes, Ekaterina Merkurjev, and Guo-Wei Wei. Graph-based bidirectional transformer decision threshold adjustment algorithm for class-imbalanced molecular data. *Journal of Computational Biophysics and Chemistry*, page Accepted, 2024.
- [52] Li Shen, Hongsong Feng, Yuchi Qiu, and Guo-Wei Wei. Svsbi: sequence-based virtual screening of biomolecular interactions. *Communications Biology*, 6(1):536, 2023.